

Molecular dynamics simulation of an evaporating sodium droplet

Anil P. Bhansali^a, Yildiz Bayazitoglu^{**}, Shigeo Maruyama^b

^a Department of Mechanical Engineering and Materials Science, Rice University,
6100 South Main Street, Houston, TX 77005-1892, USA

^b Department of Mechanical Engineering, The University of Tokyo, 7-3-1 Hongo, Bunkyo-ku, Tokyo 113, Japan

(Received 23 January 1998, accepted 3 June 1998)

Abstract—Developments and advancements have recently been made on the nanoscale level, particularly in the area of the thermal sciences. Since continuum mechanics fail in such phenomena, a demand for molecular level analysis has been created. Molecular dynamics simulation has proven to be a viable means of microscopic analysis, due primarily to the advanced design of high speed computers. A molecular dynamics simulation is performed to analyse the limits of macroscopic behaviour of an isolated evaporating liquid sodium droplet. Lennard-Jones 12-6 potential is used to determine the intermolecular forces. Details of the simulation are presented as well as variations in properties obtained from the simulation. Parameters such as the bulk liquid density, vapour density, vapour pressure, surface tension, and interfacial surface thickness with respect to temperature are determined. Comparisons of the simulation results to the limiting macroscopic properties are made and trends in the data are discussed. © Elsevier, Paris

molecular / droplet / evaporation / phase change / simulation

Résumé—Simulation de l'évaporation d'une gouttelette de sodium par la dynamique moléculaire. Des développements importants ont été réalisés récemment à l'échelle nanométrique, particulièrement dans le domaine de la thermique. Puisque la mécanique du continuum fait défaut pour l'étude de tels phénomènes, une demande pour une analyse à l'échelle moléculaire a vu le jour. La simulation par la dynamique moléculaire s'avère un moyen efficace pour une analyse microscopique, grâce principalement aux performances des ordinateurs à haute vitesse de calcul. Dans cette étude, on effectue une simulation par la dynamique moléculaire, dans le but de cerner les limites d'un comportement macroscopique d'une gouttelette isolée de sodium liquide en évaporation. On utilise le potentiel 12-6 de Lennard-Jones pour déterminer les forces intermoléculaires. Les détails de la simulation, de même que les variations des propriétés obtenues de la simulation, sont présentés. On détermine, en fonction de la température, des paramètres tels que la densité du liquide, la densité de la vapeur, la tension de vapeur, la tension superficielle ou l'épaisseur de la surface interfaciale. Des comparaisons entre les résultats de la simulation et les propriétés macroscopiques limitatives sont présentées et les tendances obtenues sont interprétées. © Elsevier, Paris

moléculaire / gouttelette / évaporation / changement de phase / simulation

Nomenclature

$B(T)$	2 nd virial coefficient
d_s	thickness of the interface
F_i	force on atom i N
k_B	Boltzmann constant ($1.381 \cdot 10^{-23}$ J)
m_a	mass of sodium atom ($3.82 \cdot 10^{-26}$ kg)
M	molecular weight of sodium (22.99 kg·mol ⁻¹)
N	number of atoms in the simulation

$N(r)$	number of atoms per spherical shell	
$P(r)$	local pressure within the droplet	MPa
P^*	reduced pressure ($= P\sigma^3/\varepsilon$)	
\bar{R}	universal gas constant	$\text{kJ} \cdot \text{mol}^{-1} \cdot \text{K}^{-1}$
r	magnitude of the radial position as measured from the centre of the drop	Å
r^*	reduced position as measured from the centre of the drop ($= r/s$)	
r_c	cut-off radius used in neighbour list routine	Å
r_e	equimolar radius	Å

* Correspondence and reprints.
bayaz@rice.edu

r_L	neighbour list radius in neighbour list routine
r_{ij}	magnitude of the distance between atom i and atom j
r_0	coefficient in the tanh curve fit (equation (7))
r_s	radius of tension
T	temperature
T^*	reduced temperature ($= k_{\text{BT}}/\varepsilon$)
v	velocity
v^*	reduced velocity ($= v/\sqrt{\varepsilon/m_a}$)
$v(r)$	volume of spherical shells used in density and pressure tensor calculations \AA^3
V	volume of the simulation box

Greek Symbols

δ	Tolman's length parameter
Δr	width of spherical shells
Δt	timestep
Δt^*	dimensionless timestep ($\Delta t/\sigma\sqrt{m_a/\varepsilon}$)
ε	depth of the potential well
γ	surface tension
$\phi(r), \phi$	potential function
$\rho(r)$	local density
ρ^*	reduced density ($= N\sigma^3/V$)
σ	first zero crossing of the potential

Subscripts/Superscripts

act	actual
i	with reference to atom i
j	with reference to atom j
k	with reference to a co-ordinate direction
K	kinetic term of the normal pressure tensor
l	liquid phase
new	scaled velocity component
p	set point
U	configurational term of the normal pressure tensor
v	vapour phase
∞	assuming infinite radius of curvature

1. INTRODUCTION

Recent developments in nanoscale phenomena, both spatially and in time, have led to an increasing number of studies dealing with small scale behaviour. Nanoscale processes must be understood on an atomic or molecular level and then related to the macroscale system of relevance. Advances, particularly in the thermal science areas, have created this demand for molecular level analyses. Kaltz et al. [1] have described the need to study the evaporation of droplets at supercritical conditions as it relates to combustion in cryogenic

	\AA
	K
	$\text{m}\cdot\text{s}^{-1}$
	\AA^3
	\AA
	\AA
	s
	J
	$\text{N}\cdot\text{m}^{-1}$
	J
	$\text{kg}\cdot\text{m}^{-3}$
	\AA

rocket motors on a microscale basis. Kotake [2] has documented the need for microscale analysis in heat pipe design, laser applications for material processing, and thermal treatment of metal castings, while Matsui and Matsumoto [3] have given much attention to rarefied gas flows on a nanoscale level. In particular within the metallurgical industry, an emphasis has been placed on the nanoscale behaviour of metals because of their relevance in metal powder production via nucleation from a supersaturated vapour, chemical vapour deposition processes, and the crystallisation of various polymers.

Since liquid metals are evident in many diverse nanoscale processes, it has become important to understand these processes on a nanoscale level. As early as 1952, attention has been focused on the need for understanding the kinetics of nucleating vapour [4, 5]. Pound [6] observed the nucleation of various types of vapours and approximated that the critical nuclei consisted of only between 80 and 100 atoms. For drops this small, statistical theory predicts a deviation in the behaviour of such droplets from macroscopic or continuum analyses. Hill et al. [7] confirmed this notion in their study of nucleating metal vapours by noting that the surface tension could be in substantial error since drops of critical size have such small radii of curvature. Nucleation phenomena are small in spatial extent in that the critical radii of the nuclei have been found to be of the order 10^{-9} m [8]. Furthermore, the time required for formation of critical nuclei has been documented to be of the order of 10^{-10} s [9].

Molecular dynamics simulations have become viable as a tool for analysing systems on a nanoscale level. This can be attributed primarily to the advanced design of high speed computers. Molecular dynamics formulations are deterministic and consist of solving Newton's equations of motion for each particle to determine properties of the material. Recently, molecular dynamics simulations have been used to investigate the molecular mechanism that governs many heat transfer processes such as the evaporation and condensation at liquid surfaces [10–12], rarefied gas interaction with a solid wall [3], conduction phenomena in thin films [13], and cluster formation and growth [12, 14–16]. The monatomic molecular dynamics is simulated by Xu, Xiong and Tzou [17] by transformation relationships between one dimension to three dimension. The thermal energy transfer near the critical point of Xenon has been analysed by Ishii, Masuda and Maekawa [18] using molecular dynamics simulation. Hydrogen bond in water is analysed over a wide range of temperatures and densities by Ohara and Aihara [19]. In the present investigation, a molecular dynamics simulation is employed to investigate the interfacial phenomena and to determine properties of an evaporating liquid metal droplet. Details of the simulation will be presented in the following section.

Molecular dynamics simulations consist of four major phases: (i) the construction of an adequate potential

that governs the intermolecular forces acting between the individual particles; (ii) the initialisation of the simulation and run parameters; (iii) the calculation of the molecular trajectories and velocities of each particle during simulation, and (iv) the analysis of the trajectories and velocities to determine the physical properties of the system (next section).

In simulating the sodium molecules the well-known Lennard-Jones 12-6 potential (*figure 1*) is used,

$$\phi(r_{ij}) = 4\epsilon \left[(\sigma/r_{ij})^{12} - (\sigma/r_{ij})^6 \right] \quad (1)$$

where r_{ij} is the separation distance between atoms i and j , σ is the first zero of the potential (3.24 Å), and ϵ is the depth of the potential well (8.27·10⁻²¹ J). The Lennard-Jones potential exhibits a short range repulsion for separation distances less than σ and long range attraction for distances greater than σ . This potential was selected because of its ease of applicability, but it could possibly have its limitations in modelling liquid metals such as sodium, because of the short-range oscillatory behaviour which liquid metals display.

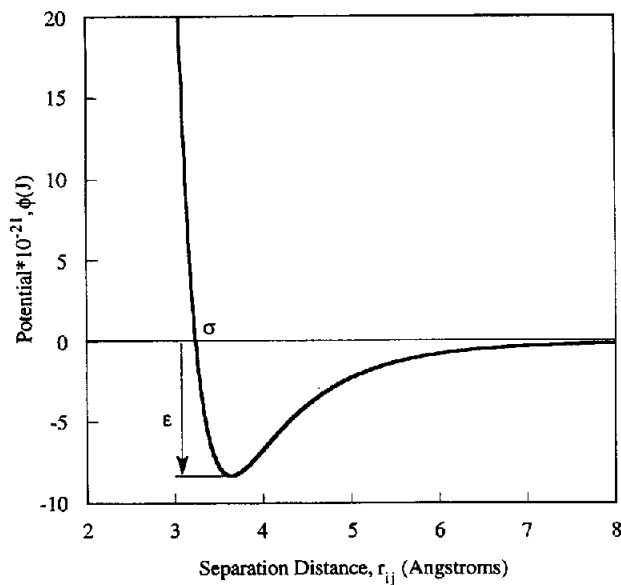


Figure 1. Lennard-Jones potential (sodium).

Initialisation of the simulation is dependent on the actual system being considered. Since it was the intent of this study to investigate thermal characteristics of an isolated evaporating liquid sodium droplet at various temperatures, a microcanonical ensemble was employed in which the number of particles, the volume, and the total energy of the system were the constrained constants [20]. A cubic simulation box served as the control volume which contained 864 sodium atoms with the walls of the simulation box replaced with cubic

periodic boundary conditions (Allen and Tildesley [22]). The size of the simulation box was chosen sufficiently large such that the periodic boundaries did not interfere with the drop (Thompson et al. [21]). The length of the box was therefore chosen to be 80 Å. The simulation was initiated with each atom occupying a position of a perfect face-centre cubic (fcc) lattice structure in a liquid state at a temperature slightly over the fusion temperature. While other initial configurations such as a body-centred cubic (bcc) lattice exist, the fcc structure is quite adequate for simulations such as the one in this study in which abnormally high densities are not considered [20]. Each atom was arbitrarily assigned a velocity in each co-ordinate direction (v_{ik}^*) via a random number generator and then scaled to the set point temperature, T_p^* , as

$$v_{ik}^{*\text{new}} = v_{ik}^* \sqrt{T_p^*/T_{\text{act}}^*} \quad (2)$$

where subscript i corresponds to a particular atom, subscript k represents the co-ordinate direction, and T_{act}^* is the actual temperature of the system determined from

$$T_{\text{act}}^* = \frac{1}{3N} \sum_i \sum_k v_{ik}^* v_{ik}^* \quad (3)$$

The variables in the simulation were normalised with respect to the standard parameters used in typical soft-sphere models and are denoted as such with the * superscript [21, 22].

In order to solve for the molecular trajectories and velocities, it was necessary to choose a suitable numerical integrator to solve Newton's equations of motion. Since no dissipative external forces exist and since the potential was assumed pairwise additive, the force on each particle could then be related to the potential in the following manner:

$$\vec{F}_i = - \sum_i \nabla \phi(r_{ij}) = m \frac{\partial^2 \vec{r}_i}{\partial t^2} \quad (4)$$

A 5th order Gear predictor-corrector algorithm was used to solve the equations of motion. This algorithm was found to have superior energy conservation characteristics to the other algorithms considered for this problem, such as the Verlet or Beeman algorithms [23, 24].

The simulation was governed by the temperature control scheme employed in the simulation as shown in *figure 2*. An equilibration period was specified at each set point temperature (T_p^*) during which the velocity was scaled according to equation (2). The length of the equilibration periods are indicated by the shaded boxes in *figure 2*.

Thermal equilibration was monitored by using a nearest neighbour routine that tracked the number of vapour atoms with respect to time. Each atom was classified as vapour, liquid, or surface depending on the number of atoms that are within a sphere of radius 1.5 σ centred at that particular atom. An atom was

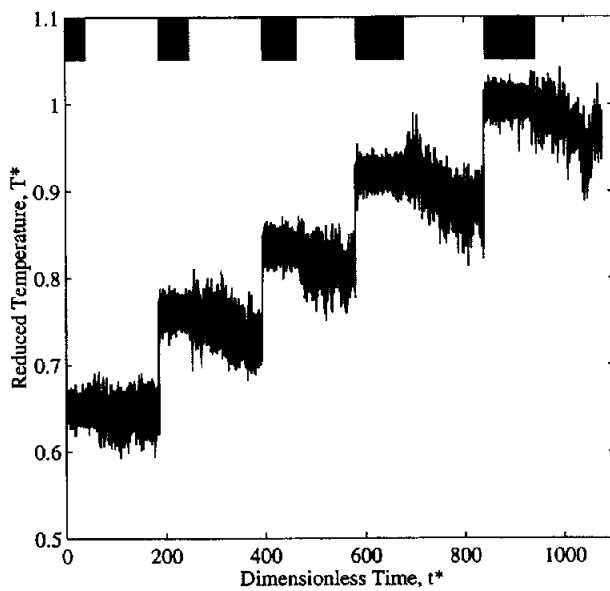


Figure 2. Temperature control strategy.

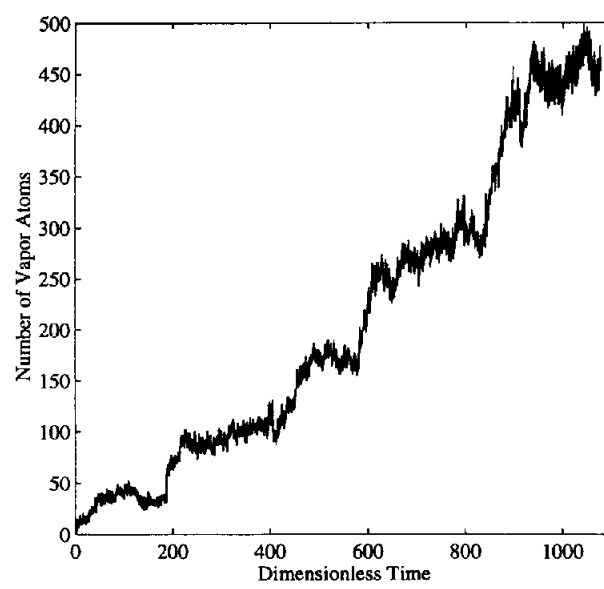


Figure 3. Vapour atom count as a function of time.

considered vapour if it had 1–2 neighbours, interfacial if it had 3–7 neighbours, and liquid if it had 8 or more neighbour atoms [25]. Thermal equilibrium had been reached when the number of vapour atoms had become relatively constant, as indicated in figure 3.

The velocity scaling was then terminated and the system was allowed to proceed in a state of constant total energy during which the trajectories and velocities were accumulated for the subsequent determination of the physical properties. The set point temperature was then reset and thermal equilibrium was then achieved at the new desired state. The dimensionless timestep used in the simulation was $\Delta t^* = 0.00144$ ($\Delta t \sim 10^{-15}$ s). The equilibration period became increasingly longer as the set point temperature of the system was increased and it consisted of up to 70 000 timesteps.

To expedite the simulation run time, a Verlet neighbour list routine was implemented [26–28] to calculate the force on each atom. For a system of N atoms, there are $N(N - 1)/2$ possible force interactions and the calculation of these interactions is extremely time-consuming. Hence, a truncated potential was used such that the force for separation distances greater than a critical cut-off distance, r_c , equals zero. Then for each atom, the routine maintains a list of neighbouring atoms that lie within a distance r_L of that particular atom where typically $r_L = r_c + 0.3\sigma$. The neighbour list for each particle was automatically updated based on a maximum particle displacement criterion, as reported by Verlet.

2. PROPERTY EVALUATION

Once thermal equilibrium had been reached at a desired temperature, the density profile throughout the drop could be calculated by determining the number of atoms in differential spherical shells of equal width, $\Delta r = 0.1\sigma$, through the following equation:

$$\rho(r) = \langle N(r) \rangle / v(r) \quad (5)$$

where $\langle \cdot \rangle$ denotes an ensemble average taken over the duration of the simulation for which thermal equilibrium exists. The shell volume is simply represented by:

$$v(r) = \frac{4\pi\Delta r}{3} (3r^2 + \Delta r^2/4) \quad (6)$$

where r denotes the midpoint of the shell as measured from the centre of the drop. The centre of the drop coincided with the center of the simulation box because the centre of mass of the drop was recalculated at each time step to compensate for any bulk motion of the drop. A regression analysis was then performed used [21] to fit the density data with the commonly used hyperbolic tangent function such that:

$$\rho(r) = \frac{1}{2} (\rho_\ell + \rho_v) - \frac{1}{2} (\rho_\ell - \rho_v) \tanh \left[\frac{2(r - r_0)}{d_s} \right] \quad (7)$$

where ρ_ℓ and ρ_v are the liquid density at the centre of the drop and vapour density at the boundary of the container, respectively, and r_0 is an estimate of the drop radius. The parameter d_s is a measure of

the thickness of the surface layer about the equimolar plane at $r = r_0$. It was also necessary to calculate the equimolar radius, r_e , as well as the radius of surface of tension, r_s , since both variables were needed in the determination of the surface tension. The surface tension can be approximated through the well-known Laplace equation:

$$\gamma = \frac{(P_\ell - P_v)r_s}{2} \quad (8)$$

where P_ℓ and P_v represent the normal components of the liquid pressure within the drop and the vapour pressure well displaced from the centre of the drop, respectively. The equimolar radius was approximated as:

$$r_e = \left[\frac{m_a N - \rho_v V}{4\pi(\rho_\ell - \rho_v)/3} \right]^{1/3} \quad (9)$$

where m_a is the mass of one sodium atom ($3.82 \cdot 10^{-26}$ kg) and V is the volume of the simulation box. r_e is defined such that if the limiting densities of two phases were constant up to $r = r_e$ and changed discontinuously at $r = r_e$. Having determined r_e via equation (9), r_s could be calculated using equation (10), which is a rearrangement of equation (8) and the Tolman equation given by equation (16) [21]:

$$r_s = \frac{3\gamma_\infty - [9\gamma_\infty^2 - 4\gamma_\infty r_e(P_\ell - P_v)]^{0.5}}{P_\ell - P_v} \quad (10)$$

where γ_∞ is the surface tension in the macroscopic or planar limit (i.e. infinite curvature).

The liquid and vapour pressures were determined via calculation of the Irving–Kirkwood pressure tensor [29]. Only the normal component of the pressure tensor, $P_N(r)$, was determined, since the calculation of the surface tension requires only this component. A detailed description of the methodology is provided by Thompson et al. [21], so only the major points will be highlighted here. The normal component can be written as the sum of kinetic, $P_K(r)$, and configurational, $P_U(r)$, contributions:

$$P_N(r) = P_K(r) + P_U(r) \quad (11)$$

where the kinetic term is given by

$$P_K(r) = k_B T_{act} \rho(r)/m_a \quad (12)$$

The evaluation of the kinetic component is straightforward and can be obtained solely from knowledge of the temperature and density profile [equation (7)] at a given instant.

The configurational contribution can be written as

$$P_U(r) = -\frac{1}{4\pi r^3} \sum_k |\vec{r} \cdot \vec{r}_{ij}| \frac{1}{|\vec{r}_{ij}|} \frac{d\phi(r_{ij})}{dr_{ij}} \quad (13)$$

where \vec{r}_{ij} is a vector between any two atoms along which the force between the two particles acts and ϕ is the pair

potential as defined by equation (1). It was possible for this vector to intersect the surface of any of the various spherical shells that were used in the evaluation of the density profile. Any intersection with a shell results in a contribution of the normal pressure to that particular shell, where each shell is defined by r , the radial distance from the centre of the drop. The scalar value of each force interaction that was positive was repulsive while any value that was negative was attractive. A hyperbolic tangent function, similar to equation (7), was used to fit both the repulsive and attractive components of the configurational terms separately. These terms will be discussed more in detail in the following section. It should be noted that the tanh fit for both the kinetic term and the configurational term was a result of time averaged data over 70 000 timesteps in the equilibrium state. The liquid pressure could then be determined in the limit of r as

$$P_\ell = P_N(r \rightarrow 0) \quad (14)$$

The vapour pressure was determined using two different methods. The first method involved direct calculation of the virial during the simulation. The second method included the use of the well-known virial equation as derived from kinetic theory

$$P_v = \frac{\rho_v \bar{R} T}{M} \left[1 + \frac{B(T) \rho_v}{M} \right] \quad (15)$$

where \bar{R} is the ideal gas constant, M is the molecular weight of sodium, and $B(T)$ is the second virial coefficient which is a function of temperature only [30]. Equation (15) incorporates the correction to the ideal gas relation such that the volume of the vapour does not approach zero as the absolute temperature approaches zero for finite pressures, since the molecules occupy some finite volume regardless of the temperature. The virial coefficient, $B(T)$ is related to the two force functions of the Lennard–Jones potential [31], since the virial coefficients can be expressed in terms of molecular forces from statistical mechanics, and evaluated upon the selection of the potential function.

3. DISCUSSION

It was necessary to validate the accuracy of the molecular dynamics model. This was accomplished by comparing with data in the published literature. Figure 4 represents a plot of the reduced potential energy and the reduced pressure (virial) obtained from the current model as well as the average values for an identical simulation performed by Haile [23]. The particular simulation was performed at a reduced density, $\rho^* = 0.6$, and a reduced temperature, $T^* = 1.54$, using a Lennard–Jones potential. Excellent agreement between the two simulations is evident as the properties obtained from the current model fluctuate precisely about the average values given by Haile [23].

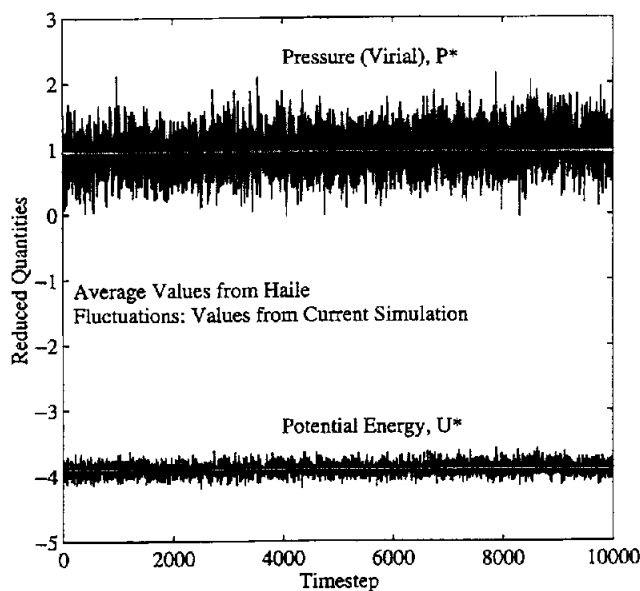


Figure 4. Comparison to Haile's data.

The focus of this work was to investigate the limits of macroscopic behaviour of an isolated evaporating sodium droplet by using molecular dynamics simulations. Thermal properties of both the bulk liquid as well as the surrounding vapour medium at various temperatures were determined. Figure 5 depicts this evaporation process. The temperatures investigated ranged from 380 to 600 K. The thermal properties are summarised in the table.

The simulation was initiated from a perfect fcc lattice structure and given initial random velocities. As was previously discussed, the thermal equilibration for each state point consisted of anywhere between 30 000–70 000 timesteps (see figure 2) which was followed by 10 000 timesteps of relaxation and 70 000 timesteps of production simulation during which properties for time averaging were accumulated. Thermal equilibrium was monitored by determining the number of vapour atoms in the system at periodic intervals as was previously discussed. The relatively flat plateaux seen in figure 3, in which the number of vapour atoms is relatively constant, represent the equilibrium periods which are associated with a constant total energy, as shown in figure 6.

The density profile data along with the hyperbolic tangent fit for each state point is shown in figure 7. It can readily be observed that the tanh fit correlates well with the data. However, the data near the centre of the droplet display a great deal of fluctuation due to the fact that the spherical shells used in the density calculations [equations (5) and (6)] become very small as the centre of the drop is approached. As expected, the liquid density of the droplet decreases as the temperature increases, while the vapour density exhibits the opposite trend.

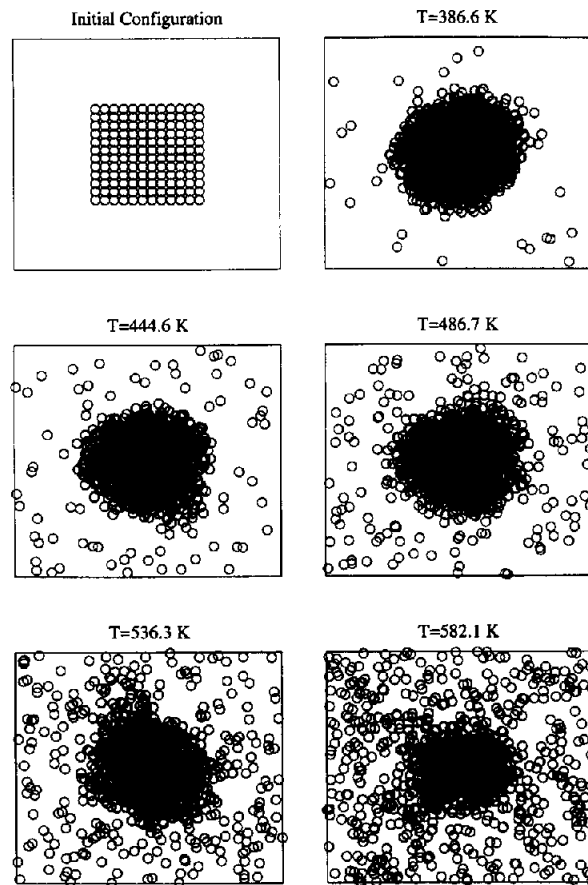


Figure 5. Schematic of the evaporation process.

It can also be observed from figure 7 that the interface between the liquid and the vapour is much more distinct at lower temperatures. But, as the temperature increases, the interface experiences a gradual spreading. As a result, the surface thickness exhibits a rapid increase. Thompson et al. [21], however, concluded in their comparison to the work performed by Powles et al. [32], that the length of the cut-off radius could significantly affect the values of the surface thickness values and that special attention should be given to such values if extremely low cut-off values are used.

The macroscopic limiting values for the liquid density corresponding to the values obtained in simulation shown in the table are 923.3, 909.6, 899.6, 887.9, 877.1 kg m⁻³, respectively, from lowest to highest temperature. For lower temperatures, the data over predicts the macroscopic limit, but as the temperature continues to increase (as the droplet shrinks), the data crosses below the macroscopic limit. This trend was also observed by Thompson et al. [21]. They attributed the decrease below the macroscopic limit to

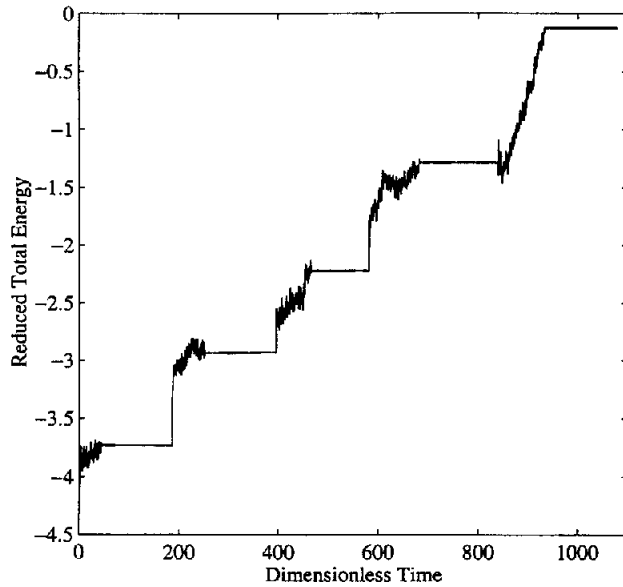


Figure 6. Total energy versus time.

a gradually decreasing cohesion within the drop as the size decreased. However, this trend was not observed by Maruyama et al. [25] in their study of an evaporating argon droplet.

The profiles of the configurational term of the normal pressure tensor, $P_U(r)$, defined in equation (13), are shown in figure 8 for the two extreme temperatures. It was previously stated that the configurational term was divided into a repulsive component for positive force interactions and an attractive component for negative force interactions. The profile of the kinetic term of the pressure tensor, $P_K(r)$ mirrors the density profile [see equation (12)] and is therefore not reproduced. A hyperbolic tangent function was again used to fit the data for both repulsive and attractive components and the limiting values ($r \rightarrow 0$) were obtained by equation (14). The repulsive component profiles, attributed to short range interactions, display more uncertainty near the centre of the drop, than its attractive counterparts, attributed to longer range interactions, due primarily to the fact that fewer short range interactions exist which makes the averaging process less reliable. The vapour pressure determined from the simulation is compared to the macroscopic bulk values as a function of temperature, as shown in figure 9. While both methods for determining the vapour pressure compare quite well with each other, they both over predict the macroscopic bulk values at lower temperatures but seem to approach the macroscopic limit as temperature increases.

The limiting macroscopic values of the surface tension data corresponding to the values obtained from the simulation via Laplace's equation [equation (8)] are 0.062, 0.051, 0.054, 0.032, and 0.025 N·m⁻¹ respectively

from lowest to highest temperature. The average of the two values obtained for the vapour pressure was used as the value of P_v in equation (8). The surface tension data are much lower than the planar limit which can be expected based on Tolman's pioneering work [33]. Thompson et al. [21] also observed such a deviance from the macroscopic limit with the discrepancy being much larger at smaller values of equimolar radius considered in this work. Tolman documented an expected decrease in surface tension as the radius of curvature decreased, especially in the range of drop sizes considered in this work. Tolman proposed an equation to account for the variation in the surface tension with drop size

$$\frac{\gamma}{\gamma_\infty} = 1 - \frac{2\delta}{r_s} \quad (16)$$

where δ is the difference $r_e - r_s$. Values for δ are given in the table I.

TABLE I Summary of properties from the simulation.									
$T(K)$ (T^*)	ρ_{ell} (kg·m ⁻³)	ρ_v (kg·m ⁻³)	r_e (Å)	d_s (Å)	r_s (Å)	P_ℓ (MPa)	$*P_\ell$ (MPa)	γ (Nm)	δ (Å)
386.6 (0.65)	982.7	2.1	19.8	5.1	14.8	83.4	0.24 (0.29)	0.062	5.05
444.6 (0.74)	940.5	6.6	19.6	5.9	14.2	72.6	1.06 (0.99)	0.051	5.45
486.7 (0.81)	907.2	12.8	19.2	6.8	14.2	81.1	2.10 (2.05)	0.054	4.96
536.3 (0.89)	864.6	20.1	18.6	7.8	13.3	57.0	3.84 (3.48)	0.032	5.34
582.1 (0.97)	830.6	36.7	16.2	9.4	11.4	51.1	6.66 (6.30)	0.025	4.86

* The vapour pressure obtained from the virial is listed above the vapour pressure obtained from the equation of state.

The value of the surface tension at $T = 486.7$ K strays from the monotonic decline in surface tension with respect to temperature. However, upon inspection of figure 2 again, it can be seen that the temperature experienced a gradual decrease during the production or equilibrium period for this state point. This indicates that while the data are quite good, both longer equilibration times might be needed in order to better define an equilibrium state and longer production periods might be required to make the time averaging more accurate.

As mentioned earlier, the need for molecular dynamics analyses is quite apparent in metal powder production processes, in particular, ones that involve nucleation from a supersaturated vapour. If the evaporation process described here was continued by increasing the set point temperature, then the drop would eventually evaporate and a uniform vapour state point would exist. Subsequently, if the temperature were then suddenly lowered (to model a sudden expansion process),

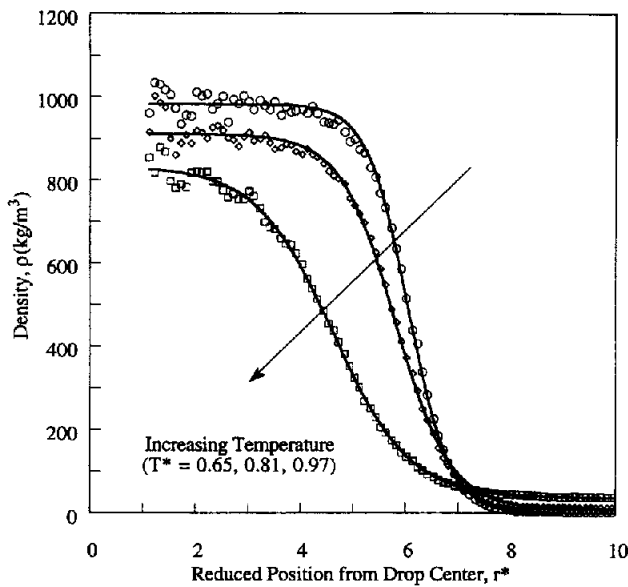


Figure 7. Density profile at various temperatures.

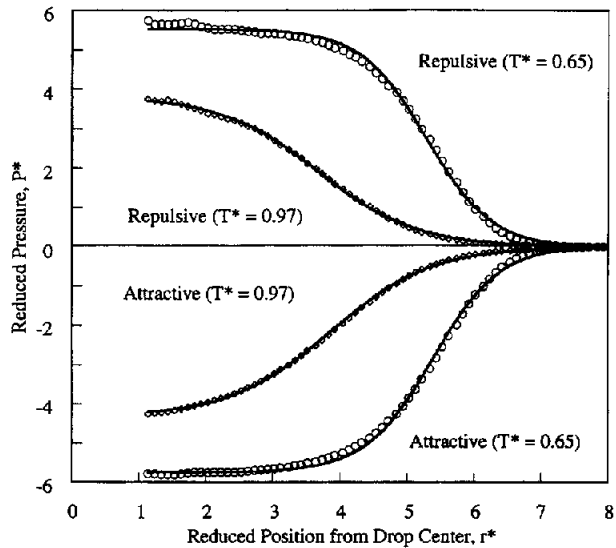


Figure 8. Reduced pressure profiles.

the vapour would exist in the thermodynamically unstable supersaturated state required for the homogeneous nucleation to initiate [34].

4. CONCLUSIONS

A molecular dynamics simulation was employed to investigate the thermal characteristics of an evaporat-

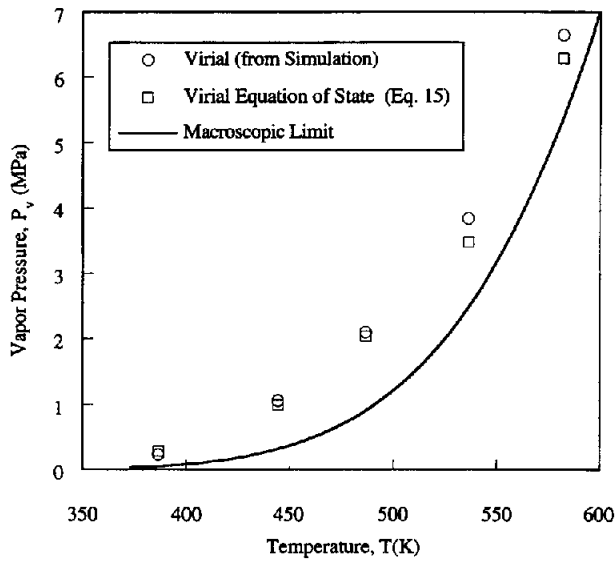


Figure 9. Vapour pressure variation with temperature.

ing sodium droplet. Various thermal properties were obtained from the simulation and compared to the limiting macroscopic values. Some of the trends in the data were also observed in the previously published literature, but there are still some questions left unresolved. While the surface tension values obtained by Maruyama et al. [25] accurately predict the macroscopic limit for argon, which is an insulator, the surface tension data obtained for sodium, a liquid metal conductor, do not reveal such a comparison. It has been well documented that the pair potentials of liquid metals exhibit an oscillatory behaviour due to ion screening which is not accounted for in the Lennard-Jones potential [35]. Since the pioneering work of Johnson et al. [36], there has been a growing interest in developing more suitable pair potentials for liquid metals [37–39]. Such potentials are now being implemented to determine their effects on the thermal behaviour of liquid metals.

Acknowledgements

This work was in part supported by Texas Advanced Technology Program under Grant No. 003604-041 and National Science Foundation under Grant No. CTS-9312379. We also acknowledge the computer time made available by the Pittsburgh Supercomputing Center.

REFERENCES

- [1] Kaltz T., Little J., Wong B., Micci M., Long L.N. Supercritical droplet evaporation modeled using molecular dynamics on parallel processors, in: Euromech Colloquium 324, The Combustion of Drops, Sprays, and Aerosols, Marseilles, France, 1994, pp. 1–9.

- [2] Kotake S., Future aspects of molecular heat and mass transfer studies, *Thermal Sci Eng.* 2 (1) (1994) 12–20.
- [3] Matsui J., Matsumoto Y., Molecular dynamics of gas-surface interaction, *ASME/JSME Thermal Engineering Proceedings* 4 (1) (1991) 59–164.
- [4] Reiss H., Theory of the liquid drop model, *Ind. Eng. Chem.* 44 (6) (1952) 1284–1288.
- [5] Michaels A.S., in: *Proceedings of Nucleation Phenomena Conference*, A Chemical Study Publications, Washington, DC, 1969.
- [6] Pound G.M., Liquid and crystal nucleations, *Ind. Eng. Chem.* 44 (6) (1952) 1278–1283.
- [7] Hill P.G., Witting H., Demetri E.P., Condensation of metal vapors during rapid expansion, *J. Heat Trans.-T. ASME* (1963) 303–317.
- [8] Lothe J., Pound G.M., Statistical mechanics of nucleation, in: Zettlemoyer A.C. (Ed.), *Nucleation*, Marcel Dekker, Inc, New York, 1969, p. 112.
- [9] Mandell M.J., McTague J.P., Rahman A., Crystal nucleation in a three-dimensional Lennard-Jones system: a molecular dynamics study, *J. Chem. Phys.* 64 (9) (1976) 3699–3702.
- [10] Yasuoka K., Matsumoto M., Kataoka Y., Evaporation and condensation at a liquid surface. I. Argon, *J. Chem. Phys.* 101 (9) (1994) 7904–7911.
- [11] Matsumoto M., Yasuoka K., Kataoka Y., Microscopic Features of Evaporation and Condensation at Liquid Surfaces: Molecular Dynamics Simulation, 1994, Vol. 2, No. 1, pp. 1–6.
- [12] Kotake S., Aoki X., Atomic and molecular clusters and their film condensation, in: *ICHMT Symposium Proceedings on Molecular and Microscale Heat Transfer in Material Processing and other Applications*, 1996, pp. 118–129.
- [13] Wakuri S., Kotake S., Molecular dynamics study of heat conduction in very thin films, *ASME/JSME Thermal Engineering Proceedings* 4 (1991) 111–116.
- [14] Rey C., Gallego L.J., Iniguez M.P., Alonso J.A., A molecular dynamics study of the evaporation of small argon clusters, *Physica B* 179 (1992) 273–277.
- [15] Nagasaki T., Hijikata K., Miyazaki K., Kaneko H., Itoh H., Fundamental study on formation of metal clusters, in: *ICHMT Symposium Proceedings on Molecular and Microscale Heat Transfer in Material Processing and other Applications*, 1996, pp. 106–117.
- [16] Sugiyama T., Echigo R., Yoshida H., Cluster formation around the critical point in two-dimensional Lennard-Jones particle system, in: *ICHMT Symposium Proceedings on Molecular and Microscale Heat Transfer in Material Processing and other Applications*, 1996, pp. 91–105.
- [17] Xu Y.S., Xiong D.X., Tzou R.D., One dimensional molecular dynamics simulation, in: *ICHMT Symposium Proceedings on Molecular and Microscale Heat Transfer in Material Processing and other Applications*, 1996, pp. 41–49.
- [18] Ishii K., Masuda S., Maekawa T., Thermofluid dynamics and molecular dynamics analyses of thermal energy transfer near the critical point, in: *ICHMT Symposium Proceedings on Molecular and Microscale Heat Transfer in Material Processing and other Applications*, 1996, pp. 58–69.
- [19] Ohara T., Aihara T., MD studies on dynamic structure of water, in: *ICHMT Symposium Proceedings on Molecular and Microscale Heat Transfer in Material Processing and other Applications*, 1996, pp. 70–80.
- [20] Rowley R.L., *Statistical Mechanics for Thermophysical Property Calculations*, PTR Prentice Hall, Englewood Cliffs, New Jersey, 1994, pp. 41 et 236.
- [21] Thompson S.M., Gubbins K.E., Walton J.P.R.B., Chantry R.A.R., Rowlinson J.S., A molecular dynamics study of liquid drops, *J. Chem. Phys.* 81 (1) (1984) 530–522.
- [22] Allen M.P., Tildesley D.J., *Computer Simulation of Liquids*, Clarendon Press, New York, 1987, pp. 17 et 87.
- [23] Haile J.M., *Molecular Dynamics Simulation*, John Wiley & Sons, Inc., New York, 1994, pp. 147–176 & 231.
- [24] Amini M., Fincham D., Evaluation of temperature in molecular dynamics simulation, *Comput. Phys. Commun.* 56 (1990) 313–324.
- [25] Maruyama S., Matsumoto S., Ogita A., Surface phenomena of molecular clusters by molecular dynamics method, *Thermal Sci. Eng.* 2 (1) (1994) 77–84.
- [26] Verlet L., Computer experiments on classical fluids. I. Thermodynamic properties of Lennard-Jones Molecules, *Phys. Rev.* 159 (1967) 98–103.
- [27] Arnold A., Mauser N., An efficient method of bookkeeping next neighbours in molecular dynamics simulations, *Comput. Phys. Commun.* 59 (1990) 267–275.
- [28] Chialvo A.A., Debenedetti P.B., On the performance of an automated verlet neighbor list algorithm for large systems on a vector processor, *Comput. Phys. Commun.* 64 (1991) 15–18.
- [29] Tsai D.H., The Virial Theorem and Stress Calculation in Molecular Dynamics, *J. Chem. Phys.* 70 (1979) 1375.
- [30] Reed T.M., Gubbins K.E., *Applied Statistical Mechanics*, McGraw-Hill, New York, 1973, pp. 202–207.
- [31] Hirschfelder J.O., Curtiss C.F., Bird R.B., *Molecular Theory of Gases and Liquids*, John Wiley & Sons, New York, 1964.
- [32] Powles J.G., Fowler R.F., Evans W.A.B., A new method for computing surface tension using a drop of liquid, *Chem. Phys. Lett.* 98 (1983) 421–426.
- [33] Tolman R.C., The effect of droplet size on surface tension, *J. Chem. Phys.* 17 (1949) 333–337.
- [34] Stever H.G., *High Speed Aerodynamics and Jet Propulsion*, Section F., Princeton University Press, 1954, pp. 532–536.
- [35] Ashcroft N.W., Mermin N.D., *Solid State Physics*, Holt Rinehart and Winston, New York, 1976, pp. 337–345.
- [36] Johnson M.D., Hutchinson P., March N.H., Ion-ion oscillatory potentials in liquid metals, *P. Roy. Soc. Lond. A* 282 (1964) 283–302.
- [37] Price D.L., Shyu W., Singwi K.S., Tosi M.P., Argonne National Report, ANL 7761, 1970.
- [38] March N.H., Structure and Forces in Liquid Metals and Alloys, *Can. J. Phys.* 65 (1987) 219–240.
- [39] Rani M., Pratap A., Saxena N.S., Single Particle and Collective Motions in Liquid Rubidium, *Ind. J. Pure Appl. Phys.* 27 (1989) 269–274.